Journal of Structural Geology, Vol. 9, No. 2, pp. 207 to 219, 1987
Printed in Great Britain

0191-8141/87 $03.00 + 0.00

Geometric analysis of fold development in overthrust terranes

WILLIAM R. JAMISON

Amoco Production Company, P.O. Box 3385, Tulsa, OK 74102, U.S.A.

(*Received* 16 *July* 1985; *accepted in revised form* 30 *June* 1986)

Abstract—Fault-bend folding, fault-propagation folding, and detachment (or décollement) folding are three distinct scenarios for fold-thrust interaction in overthrust terranes. Simple kink-hinge models are used to determine the geometric associations implicit in each scenario. Bedding maintains constant thickness in the models except in the forelimb of the fold. The forelimb is allowed to thicken or thin without limit. The models address individual folds, and the calculated fold geometries are balanced structures.

Each mode of fold-thrust interaction has a distinct set of geometric relationships. Final fold geometry is adequate in itself to discern many fault-bend folds. This is not the case for fault-propagation and detachment folds. These two fold forms have very similar geometric relationships. Some knowledge of the nature of the underlying thrust or décollement zone is usually needed to distinguish between them. The geometry of a fold is altered, in a predictable fashion, by transport through an upper ramp hinge and by fault-parallel shearing of the structure. The shearing results in a tighter fold, whereas transport through the ramp hinge produces a broader fold.

The viability of the geometric analysis technique is demonstrated through its application to a pair of detachment folds from the Canadian Cordillera. The geometric analysis is also used to evaluate cross-sections through subsurface structures. In an example from the Turner Valley oil field, the analysis indicates how the interpretation should be altered so as to balance the cross-section. The analysis reveals hidden assumptions and specific inconsistencies in structural interpretations.

INTRODUCTION

ONE OF the basic functions of structural geology is the description and prediction of the geometry of naturally occurring structures. Prediction commonly consists of combining experience with some form of constraint, either conceptual, mechanical, or geometric. The constraint basically guides or justifies the predictor's intuition. This article examines a system of geometric constraints, based on the initial fold-thrust interaction, that may be used to examine individual folds in overthrust terranes.

The 'balancing' of cross-sections is certainly the most commonly utilized geometric constraint for overthrust structures. 'Balancing' is simply a test for conservation of volume. It is a check to assure that the total rock volume remains constant through the history of development of a geologic structure. Dahlstrom (1969) formally introduced the balancing procedure, and presented a set of tenets derived from his experience with structures in the southern Canadian Cordillera. The specific guidelines presented by Dahlstrom (1969) apply to regional cross-sections (e.g. Dixon 1982). They were not intended, and often are not appropriate, for the assessment of individual structures.

A construction procedure that is designed for the interpretation of individual structures as well as regional analyses is presented in Suppe (1983). Focusing on the fault-bend fold (Fig. 1a), or Rich-model mode of fold-thrust interaction (Rich 1934), Suppe derived a suite of curves relating the fold interlimb angle to upper and lower ramp angles. Similar relationships have also been derived for fault-propagation folds (Fig. 1b) (Suppe & Medwedeff 1984). While these analyses are not explicitly presented as balancing procedures, the basic tenet of balancing (conservation of volume) is the foundation behind the equations. As a consequence, a fold–thrust system that displays geometric relationships compatible with the curves and assumptions of Suppe (1983) or Suppe & Medwedeff (1984) is balanced.

In this article, a geometric analysis is presented that extends the approach of Suppe (1983) and Suppe & Medwedeff (1984). Certain of the constraints of their model are relaxed in order to permit variations in the amount or type of deformation through the fold. Detachment folds are added as a third type of thrust-associated

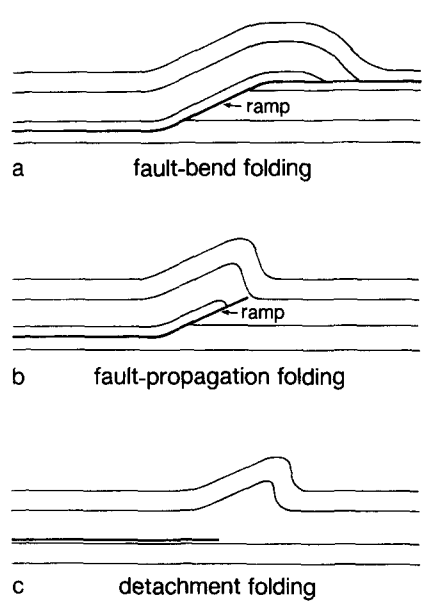

Fig. 1. Three types of fold-thrust interactions: (a) a fault-bend fold, (b) a fault-propagation fold, and (c) a detachment fold.

fold. Also, the effects of fold transport and shearing on fold geometry are considered. This analysis defines the range of geometries most probable for each mode of folding and demonstrates that the history of fold development and transport can, to a certain extent, be determined from final fold geometry. Unlike the procedures of Dahlstrom (1969), Suppe (1983) and Suppe & Medwedeff (1984), this analysis is not intended to be used for regional structural reconstructions (e.g. Suppe 1980). Rather, it is strictly a balancing guideline for individual folds in an overthrust terrane.

MODES OF FOLD-THRUST INTERACTION

Three fold forms are distinguished, viz. fault-bend, fault-propagation, and detachment (or décollement) folds (Fig. 1). For the geometric analysis, these three modes are defined simply in terms of geometry, with no kinematic or mechanical considerations. For the initial analysis, the structures are assumed to be in their early phases of development. A fault-bend fold (Fig. 1a) develops as the hangingwall of a thrust is transported through a ramp region on the thrust surface. This fold model was introduced by Rich (1934) to account for the geometry of the Pine Mountain overthrust in the southern Appalachians. The fold forms as a consequence of the movement of the hangingwall rocks through the ramp region. As a result, the forelimb of the fault-bend fold is always located on the foreland side of its associated ramp. While the fault-bend fold model has found widespread acceptance and application, in many cases it is simply, as Dahlstrom (1970, p. 361) noted, a 'convenient fiction'. Even though it is not universally appropriate, it is the easiest of the three fold-thrust forms to conceive, draw and model.

A fault-propagation fold (Fig. 1b) also has a direct association with the ramp region of the underlying thrust. Whereas the fault-bend fold develops subsequent to the ramp formation, the fault-propagation fold develops simultaneously with and immediately above the ramp. The displacement along the thrust diminishes progressively to zero along the ramp region beneath the fault-propagation fold. Stated otherwise, the fault-propagation fold develops at the termination of a thrust (Williams & Chapman 1983). The fold, in fact, is the geologic expression of the strain that implicitly must occur at a fault termination.

The detachment fold (Fig. 1c), like the fault-propagation fold, develops at the termination of a thrust. Unlike the fault-propagation fold, the detachment fold is not associated with a ramp in the underlying thrust. Rather, the detachment fold develops above a bedding detachment (or décollement), hence its name. Beneath the fold, the displacement along the detachment (bedding-parallel thrust) diminishes progressively to zero in a foreland direction.

A fold located at the tip of a blind thrust (Boyer & Elliott 1982) must be either a fault-propagation or detachment fold. The mechanical stratigraphy determines the probable fold-thrust relationship. A detachment fold might be expected where the thrust rides low in a ductile unit, that in turn underlies a more competent unit. In a layered sequence with more modest ductility contrasts, the fault-propagation fold may be more probable. (A hybrid is, of course, conceivable, maybe even common, but the geometry of that possibility is not considered here).

In both the fault-bend fold and the fault-propagation fold, the lower strata involved in the fold are truncated against the thrust. Consequently, both may be termed 'truncation anticlines'. The hangingwall truncation of the fault-bend fold lies foreland of the ramp, whereas in the fault-propagation fold it initially is on the ramp (Fig. 1). Thus the fault-bend and fault-propagation folds may be distinguished on the basis of the position, relative to the ramp, of the fold and the hangingwall truncation. However, as the fault in the fault-propagation fold grows and the fold is transported, both the hangingwall truncation and the fold are transported foreland of the associated ramp. As a result, the position of the fold and truncated beds no longer indicates the mode of fold genesis.

MODEL CONFIGURATIONS AND PARAMETERS

The analyses presented below are derived using structural models with simple kink-hinge geometries (e.g. Fig. 2b). The thickness of each stratigraphic unit remains constant throughout the structure, except in the forelimb of the fold. The forelimb can thicken or thin, but the thickness change must be constant throughout the forelimb. The kink-hinge configurations are used to simplify the geometric calculations discussed below, and are not intended to be strict representations of geological stuctures. Models with curvilinear fold hinges (e.g. Fig. 1), although aesthetically much more appealing than the angular forms, yield virtually the same angular relationships and are, geometrically, much more cumbersome.

The use of a variable forelimb thickness is a departure from most balancing procedures, wherein bedding maintains constant thickness throughout the entire structure (e.g. Dahlstrom 1969, Suppe 1983, Suppe & Medwedeff 1984). Detailed surface and subsurface studies of individual thrust-associated folds have shown, however, that the overall forelimb thickness can differ significantly from backlimb bedding thickness (e.g. Gallup 1951, Brown & Spang 1978, Williams & Chapman 1983). Small imbricate faults, minor folds or ductile flow of certain beds can produce this thickness contrast. Whereas the assumption of constant bedding thickness is probably adequate for regional sections, it can be inappropriate for the investigation of individual folds.

The solutions presented in the following section are derived for the dip cross-section of the structure. Plane strain is assumed, implying that there is no loss or gain of material into the plane of the cross-section. During fold development, geometric alterations occur only in the fold itself and in the hangingwall above the ramp. Out-

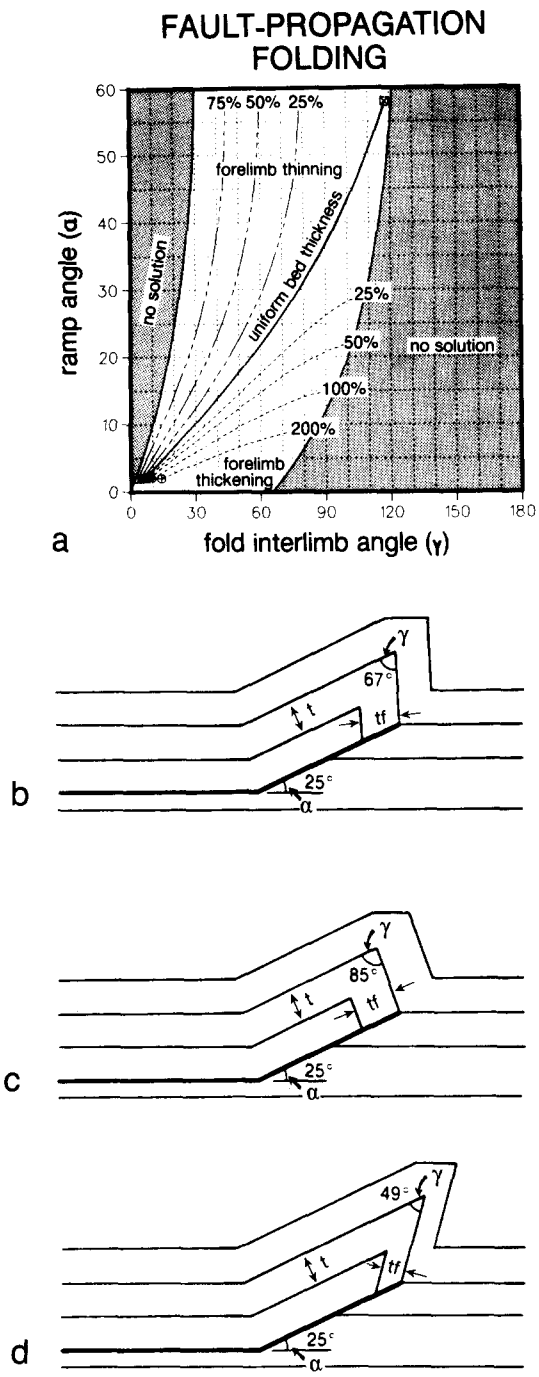

Fig. 2. Geometric analysis of fault-propagation folding. (a) Curves relating fold interlimb angle (γ) to ramp angle (α) for specified amounts of forelimb thickening and thinning. For any particular value of α, there exists a broad range of possible values for γ, depending on the amount of tectonic thickening or thinning of forelimb beds. For example, for $\alpha = 25°$, (b) a fold with uniform limb thickness has an interlimb angle of 67°, (c) a fold with 25% thickening of the forelimb has an interlimb angle of 85° and (d) a fold with 35% thinning of the forelimb has an interlimb angle of 49°.

side of this region, the hangingwall material is translated along the fault, but not altered in any other way. The footwall in all models is totally unaltered. The cross-sectional area of the material within the deformed region is equated with its undeformed area. This equality, combined with the plane strain assumption, ensures that rock volume is conserved during fold development and transport; i.e. the structures are balanced. The various geometric relationships presented in this analysis are simply the solutions to these balanced equations (see Appendix).

The interrelated parameters in the truncation anticlines are the ramp angle (α), the interlimb angle (γ), and the thickness change (tf/t) occurring in the forelimb (Figs. 2 & 3). In the detachment fold, backlimb dip (α_b) replaces ramp angle (Fig. 4). Additionally, the geometric analysis of the detachment fold requires specification of a fourth parameter, viz. the ratio of the fold amplitude (a) to the normal stratigraphic thickness (f) of the ductile unit infilling the core of the fold. As a result, the geometric relationships of the detachment fold are a direct function of the size (amplitude) of the structure. The angular relationships derived for the truncation anticlines have no dependence on fold amplitude.

Although the model configurations have been made simplistic to facilitate the calculations, the general forms are compatible with many folds observed in overthrust terranes. Faill (1969) noted that the dominant characteristics of folding in the Appalachians in Pennsylvania are planar limbs and angular hinges. Similar characteristics are evident in published examples of thrust-associated folds in Alberta (Brown & Spang 1978), British Columbia (Fitzgerald & Braun 1965), Tennessee (Serra 1977), England (Williams & Chapman 1983) and in the Jura of Switzerland (Laubscher 1977).

GEOMETRIC RELATIONSHIPS

Fault-propagation folding

Fold interlimb angle (γ) is a function of a ramp angle (α) and the amount of forelimb thickening or thinning (Fig. 2). The ramp angle for the fault-propagation fold is the angle that the ramp makes with the lower flat of the thrust. The curves relating α and γ (Fig. 2a) indicate that a fault-propagation fold with ramp angle of, say, 25° theoretically must have an interlimb angle of from 21° to 105°. If the beds maintain their original thickness throughout the fold (as in the analysis of Suppe & Medwedeff 1984), the interlimb angle is 67° (Fig. 2b). If the forelimb is thickened, the fold will have a larger interlimb angle. For the case of 25% thickening of the forelimb the interlimb angle is 85° (Fig. 2c). If the forelimb is attenuated, the fold will be tighter. A fold with 35% thinning of the forelimb beds should have an interlimb angle of 49° (Fig. 2d).

Fault-bend folding

Again, fold interlimb angle (γ) is a function of ramp angle (α) and the amount for forelimb thickening or thinning (Fig. 3). The ramp angle for the fault-bend fold is defined in terms of δ and β (Fig. 3b), the lower and upper ramp hinge angles, respectively, as

$$\alpha = \cot^{-1}\left(\cot\delta + 2\cdot\left(\tan\frac{\delta}{2} - \tan\frac{\beta}{2}\right)\right).$$

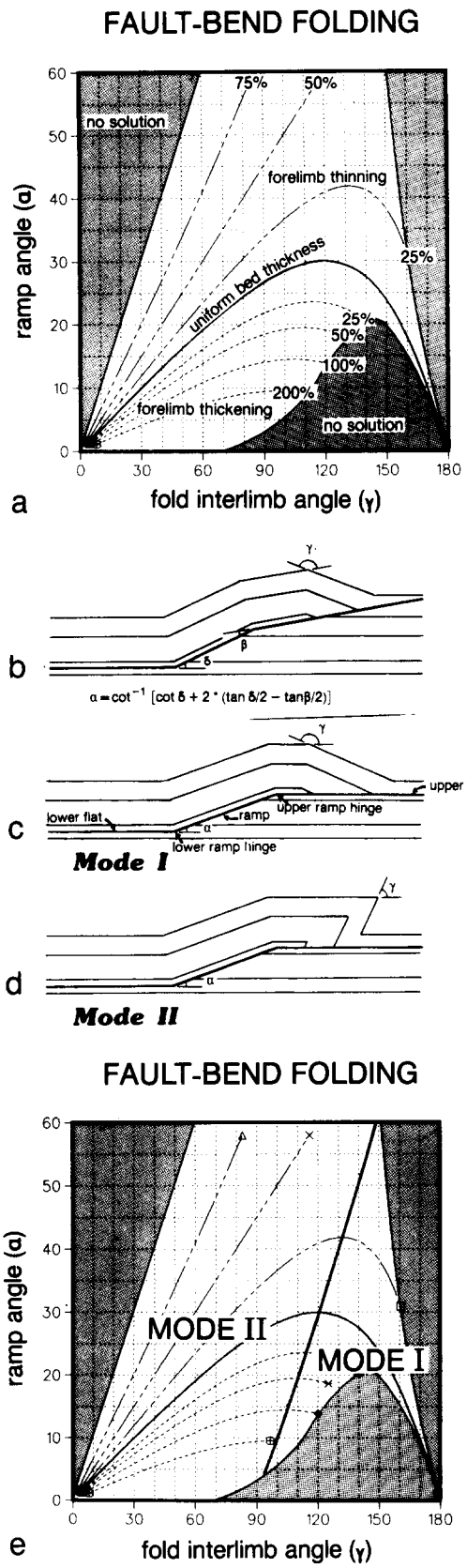

Fig. 3. Geometric analysis of fault-bend folding. (a) Curves relating fold interlimb angle (γ) to ramp angle (α) for specified amounts of forelimb thickening and thinning. Units maintain constant thickness except in the forelimb. (b) For the general case of unequal upper and lower ramp hinge angles (β and δ, respectively), an 'effective' ramp angle (α) is used to assess possible fold geometries. (c) Mode I and (d) Mode II fold geometries, following the distinction of Suppe (1983). The geometric analysis chart may be divided into domains (e) representing these two modes.

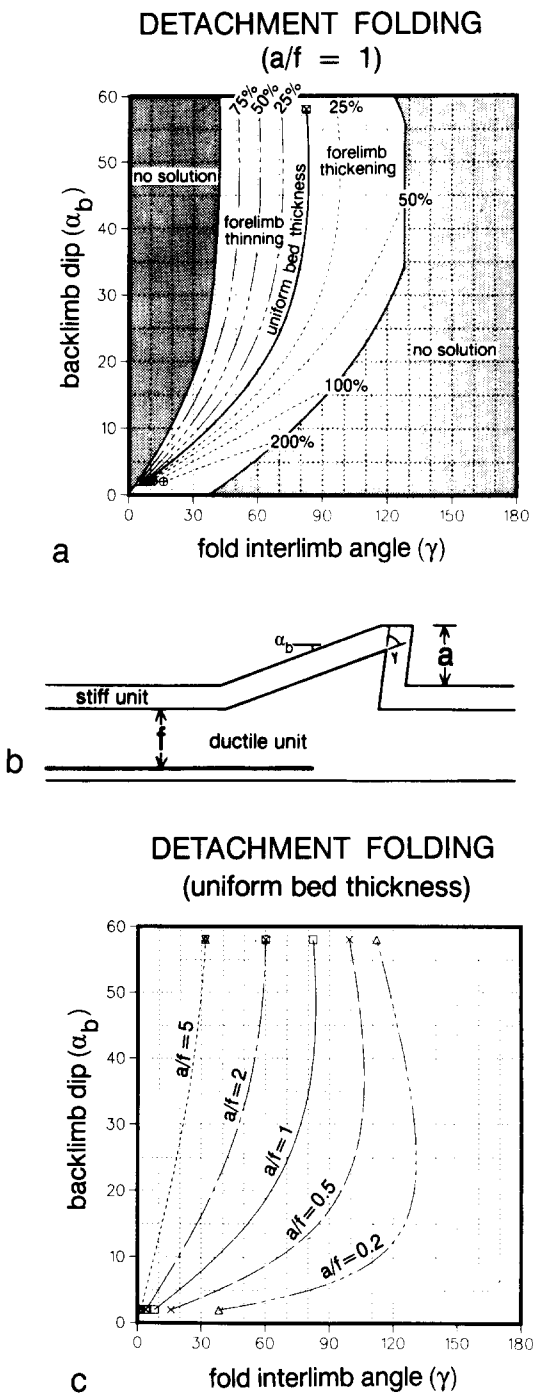

Fig. 4. Geometric analysis of detachment folding. (a) Curves relating fold interlimb angle (γ) to backlimb dip (α_b) for specified amounts of forelimb thickening and thinning, and $a/f = 1.0$. Bedding in the stiff layers maintains constant thickness except in the forelimb. (b) The detachment fold model is divided into 'stiff' and 'ductile' units. The fold form is expressed in the stiff units. The ductile units maintain constant thickness except in the region directly beneath the fold in the stiff units. (c) Curves relating γ to α_b for specified a/f values and the case of constant unit thickness in the stiff layers throughout the structure.

The most common values for both lower and upper ramp hinge angles observed in natural structures are 10–40° (Serra 1977, Boyer & Elliott 1982). Within this range $\alpha \approx \delta$. Commonly, both upper and lower 'flats' along the thrust are parallel to footwall bedding. In this case δ and β are equal, and $\alpha = \delta$.

The case of constant bed thickness through the fold was treated by Suppe (1983). He noted that there were

two possible interlimb angles for any specified ramp angle (except $\alpha = 30°$, the maximum possible ramp angle in this case). To distinguish these two solutions, Suppe (1983) specified the larger interlimb angle solution to be a Mode I fold (Fig. 3c). The smaller interlimb angle fold is a Mode II fold (Fig. 3d). This distinction between Mode I and Mode II fault-bend folds can be extended through the range of solutions made in the current analysis (Fig. 3e).

Detachment folding

For the detachment anticline (Fig. 4), a suite of curves similar to those derived for the truncation anticlines can be generated for any specified *a/f* value (Fig. 4a). Note that interlimb angle (γ) is plotted against backlimb angle (α_b), where backlimb angle is the acute angle between projected backlimb strata and the décollement surface, which is assumed to be planar and parallel to footwall bedding.

Unlike truncation anticlines, the value of α (here, α_b) for a detachment anticline will generally change as the structure develops. Also, the fold amplitude increases as the structure grows and, thus, *a/f* increases (*f* does not change). The effect of *a/f* on interlimb angle is significant (Fig. 4c). In general, γ decreases as *a/f* increases; i.e. the fold gets tighter as amplitude increases.

For a given *a/f* value, the range of possible solutions (on the γ-α plots) for the detachment fold is more limited than for either of the truncation anticlines (compare Fig. 4a with Figs. 2a & 3a). However, because the swath of possible solutions shifts as *a/f* changes, there is actually a greater range of possible geometries for the detachment anticline than for either of the truncation anticline models.

SUBSEQUENT GEOMETRIC ALTERATIONS

Transport through an upper ramp hinge

A fault-propagation fold develops above the propagating ramp of its associated, underlying thrust. If the fault subsequently flattens as it continues to propagate in a foreland direction, an upper ramp hinge is formed (Fig. 5a). The geometry of the fold is altered if the fold is transported through this new ramp hinge. In all cases the fold becomes broader (Fig. 5b). Thickening or thinning of the forelimb is dictated by the original interlimb angle of the fold and the angle of this upper ramp hinge

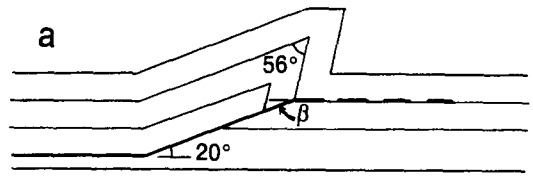

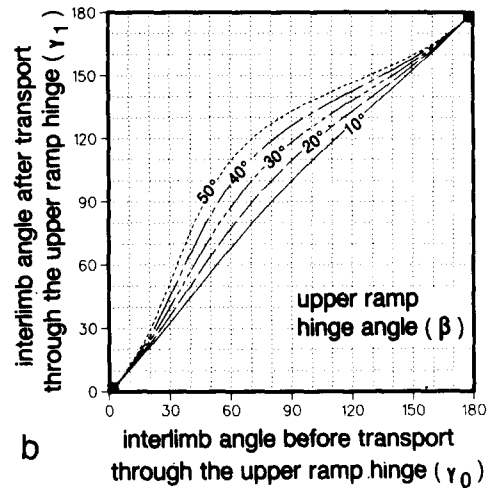

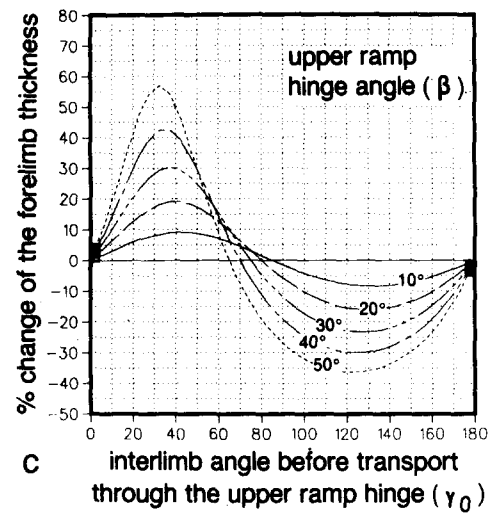

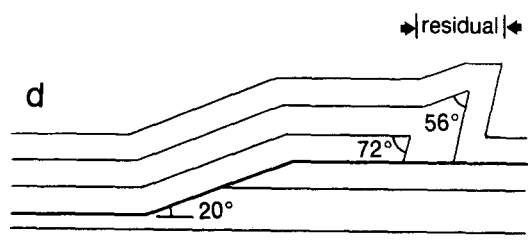

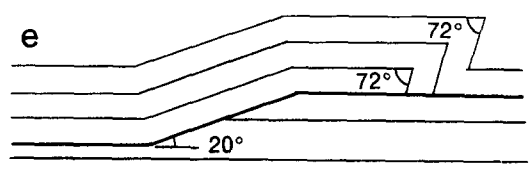

Fig. 5. (a) An upper ramp hinge develops beneath a fault-propagation fold if the underlying thrust flattens as it extends in a foreland direction. Geometric effects of transport through an upper ramp hinge upon (b) fold interlimb angle and (c) fold forelimb thickness. Transport through a lower ramp hinge would have the reverse effect. The interlimb angle of the original fold (a) is broadened by transport through the upper ramp hinge (d). The portion of the fold that does not move through the upper ramp hinge (the 'residual') maintains its initial geometry. The altered portion of the fault-propagation fold has the same geometry as a Mode II fault-bend fold with equivalent ramp angle (e).

(Fig. 5c). Only the portion of the fold that is transported through this hinge undergoes the geometric alteration. Any part of the fold that was already located foreland of the hinge is a 'residual' (Fig. 5d) that is transported without any associated geometric alteration. Roughly, the hangingwall beds that are truncated by the ramp undergo geometric alterations, whereas those beds not truncated form the residual. The residual will always have a smaller fold interlimb angle than that portion of tne fold that has been altered.

The portion of the fault-propagation fold that moves through the upper ramp hinge (Fig. 5d) is found to have a geometry that is identical to a Mode II fault-bend fold with the same ramp angle (Fig. 5e). The transport of the fold through the upper ramp hinge thus eliminates much of the geometric distinction between these two forms of truncation anticlines. For the general case, assuming that the fold is transported through an upper ramp hinge angle equal to the original ramp angle of the fold (i.e. its lower ramp angle), a suite of curves for transported fault-propagation folds may be generated (Fig. 6a). These new suites of curves coincide with the corresponding curves for the fault-bend fold model (Fig. 6b), but are effectively limited to the Mode II region of fault-bend folding.

A detachment fold may be converted into a truncation anticline if the detachment thrust, or an imbricate of this fault, cuts up-section through the forelimb of the fold. Only the portion of the fold that overlies this new ramp will be affected by subsequent transport of the fold through the upper ramp hinge. The geometric alterations can be calculated using the appropriate charts for fold transport (Figs. 5b & c). Because of the broad range of possible configurations for the original detachment fold, geometric similarities between a truncated and transported detachment fold and either a fault-propagation or fault-bend fold would be coincidental.

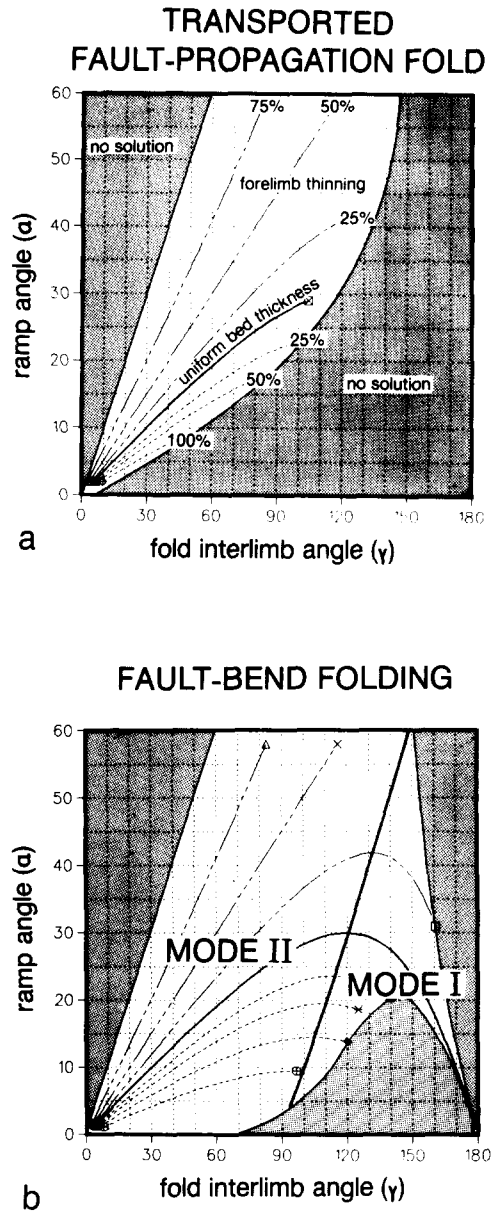

Fig. 6. Comparison of geometric relationships for (a) a fault-propagation fold transported through an upper ramp hinge of angle equal to the original ramp angle with those for (b) a fault-bend fold. The curves coincide, but the transported fault-propagation fold is essentially restricted to the Mode II domain of the fault-bend folding.

Fault-parallel shearing

In the truncation anticlines, the backlimb of the fold is parallel, or close to parallel, to the surface of the transporting thrust. In many thrust-associated folds there are suggestions that shear displacement has occurred along some of the backlimb bedding surfaces during fold development and/or transport. Such internal shearing will alter fold geometry. To assess these effects, movement on these surfaces is treated as fault-parallel shear occurring pervasively through the affected zone. Both the interlimb angle of the fold and the relative thickness of the forelimb are affected (Fig. 7).

Fault-parallel shear always reduces the fold interlimb angle (Fig. 7a). In general, this shearing will thin the forelimbs of fault-propagation folds, Mode II fault-bend folds, and most detachment folds, but will thicken the forelimbs of Mode I fault-bend folds. In nature, the existence of such bedding-plane slip is often difficult to demonstrate, and almost always impossible to measure. Thus, although the amount or even the existence of this fault-parallel shearing can seldom be directly assessed, it may be inferred indirectly via geometric analysis.

For a specified initial geometry and amount of shearing, the reduction in interlimb angle implies a change in forelimb thickness. However, the original charts for these fold models (Figs. 2–4) also associate a reduction in interlimb angle (maintaining a constant α) with a specific forelimb thickness change. Even so, the sheared fold has a geometry that is distinct from a fold that has become tighter without any associated fault-parallel shear. Specifically, for a given α and γ, the sheared fold has a thicker forelimb than an unsheared fold (compare Figs. 7d & f). This reflects the fact that the shearing process moves material into the hinge and forelimb regions of the fold.

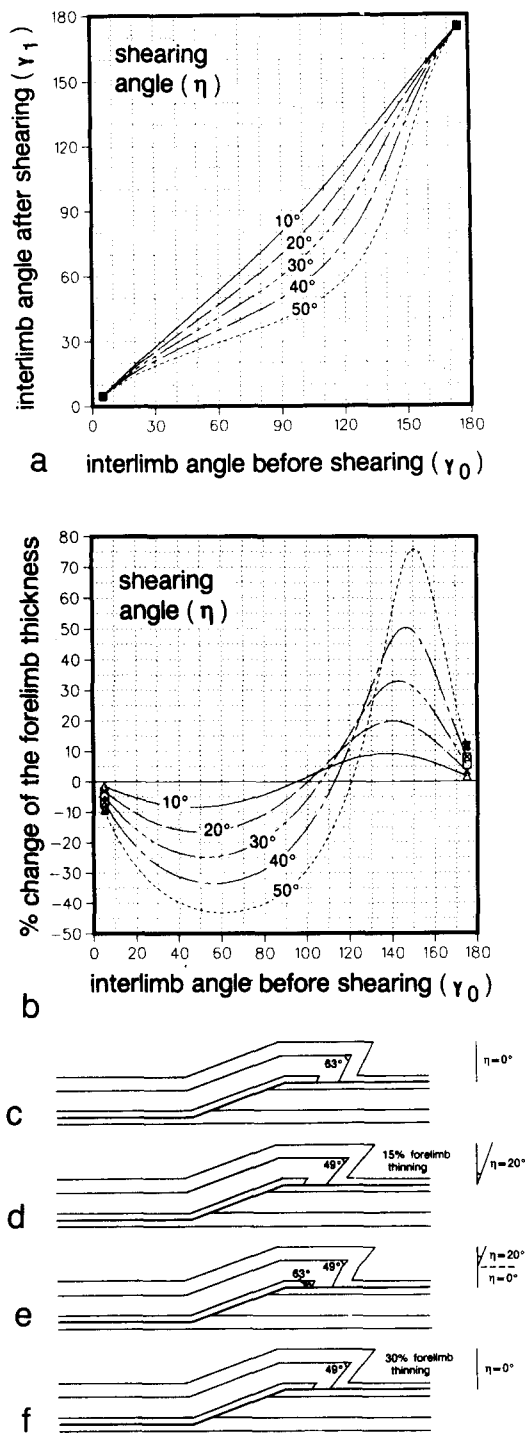

Fig. 7. Geometric effects of fault-parallel shearing on (a) fold interlimb angle, and (b) fold forelimb thickness. For the case of a Mode II fault-bend fold with $\alpha = 20°$ and uniform bed thickness, the original structure (c) may be sheared in its entirety (d) or only in part (e). An unsheared fold of similar interlimb angle (f) has a thinner forelimb than the corresponding sheared fold (d).

GEOLOGICAL INFERENCES

Although there is considerable overlap of the domains of possible solutions for the several modes of fold-thrust interaction (Figs. 2–4), some inferences regarding mode of development may be obtained directly from the final geometry of a structure. For example, most large folds with interlimb angles greater than 120° are Mode I fault-bend folds. Detachment folds that occur in this domain of large interlimb angles must have small a/f ratios (Fig. 4c), and fault-propagation folds are not geometrically viable. Subsequent tightening of a Mode I fault-bend fold, with or without fault-parallel shearing, will thicken the forelimb region. Folds with moderate interlimb angles ($80° \leqq \gamma \leqq 120°$) and substantial imbrication in the forelimb may be examples of modified Mode I fault-bend folds.

In the domain of folds with moderate to small interlimb angles, little can be inferred regarding mode of fold-thrust interaction simply from a knowledge of the interlimb angle itself. For example, the curves for a detachment fold with $a/f = 1.0$ (Fig. 4a) are very similar to those for a fault-propagation fold (Fig. 2a). Determination of interlimb angle, backlimb dip, and forelimb thickness change will not distinguish between these two forms of fault-tip folding. Only direct knowledge of the existence or nonexistence of a propagating ramp can resolve this case. On a positive note, many specific fold geometries do suggest a unique genesis. For example, a very tight, upright fold with little forelimb thinning is almost certainly a detachment fold with a high a/f ratio (Fig. 4c).

Additional inferences regarding fold genesis may be made using kinematic considerations. For the case of the fault-bend fold, the Mode I geometry is the form depicted by Rich (1934) and used in most other investigations, models, or analyses based upon the fault-bend fold model (e.g. Wiltschko 1979a,b, Morse 1977, Berger & Johnson 1980). The forelimb of the fold in Mode I is simply flexed downward as the hangingwall rock moves through the upper ramp hinge.

Conceptually, a Mode II fold must also initiate as a Mode I structure. The transition to the Mode II form occurs, in terms of the geometric charts, via a shift to the left along a constant ramp angle line (Fig. 3e). This shift requires the forelimb first to thicken and then to thin. This complex deformation path presumably would leave its mark in the form of substantial deformation of the forelimb beds. In fact, deformation might be so intense as to render bedding in the forelimb virtually unrecognizable.

If these speculations are valid, then it follows that a fold with a Mode II fault-bend fold geometry and only moderate forelimb deformation is more likely to be a transported fault-propagation fold (Fig. 6a) than a true fault-bend fold. Where specific structures are being assessed, features such as a slightly more appressed 'residual' in the non-truncated beds would add support to a fault-propagation interpretation.

APPLICATIONS

Geometric analyses of two sets of thrust-associated folds in the Canadian Cordillera serve to illustrate some of the uses and limitations of this technique. The first structure is a pair of folds, well exposed on a cliff face in northeastern British Columbia. The second is the Turner Valley Anticline, a subsurface structure whose configuration is defined by abundant well control.

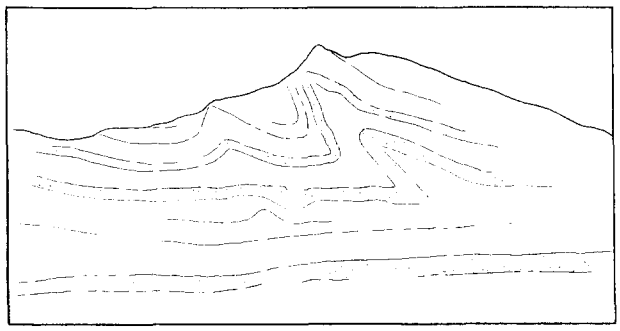

Fig. 8. Detachment anticlines in Besa River beds in northeastern British Columbia. After Fitzgerald & Braun (1965).

Outcrop example

These two folds (Fig. 8), located in the Main Ranges of the Canadian Cordillera in northeastern British Columbia, are developed in the Devonian–Mississippian Besa River Formation (Fitzgerald & Braun 1965). This formation is dominantly shale with some sandstone stringers. The folds occur above a bedding-parallel detachment surface. Direction of transport is from right to left in Fig. 8. There is no fault ramp associated with either fold; they are detachment folds in the context of this article.

The two folds appear to have developed above different detachment surfaces. The units used in a geometric evaluation must be located above zones of complex deformation that might occur in the core of the fold. In the case at hand, each fold is analyzed using the bedding units in the upper reaches of the outcrop. To assess the angular values needed in the geometric analysis, each limb of the fold, as well as the detachment surface, must be approximated by a single, straight line.

The right-hand fold (Fig. 8) is analyzed using horizon *m* (Fig. 9a). The fold interlimb angle (γ) at this horizon is 48°, the backlimb dip (α_b) measured relative to the detachment surface is 24° and the *a*/*f* value is 1.1. Note that *f* includes the entire interval between the detachment surface and horizon *m*. Consequently, the results of this particular analysis apply only to the units above horizon *m*. The geometric analysis indicates that a detachment fold with the measured angles and *a*/*f* value should exhibit a thinning in the forelimb units of about 50% (Fig. 9b). In the outcropping structure, the forelimb thickness (tf_r) is about 45% thinner than the presumed normal stratigraphic thickness (t_r).

In the left-hand fold set (Fig. 8), using horizon *k*, the fold interlimb angle (γ) is 82°, the backlimb dip (α_b) is 28°, and *a*/*f* is about 0.9 (Fig. 9c). Geometric analysis suggests a slight (5–10%) thickening should occur in the forelimb of the fold (Fig. 9d). In the outcropping structure, the upper units involved in this fold appear to have essentially uniform thickness across the fold.

The good correspondence between the geometry of naturally occurring folds and the model predictions supports the viability of the geometric analysis approach. The correlations should be good in this case, for the outcropping folds closely mimic the models used in the analysis (or vice versa). However, despite the simi-

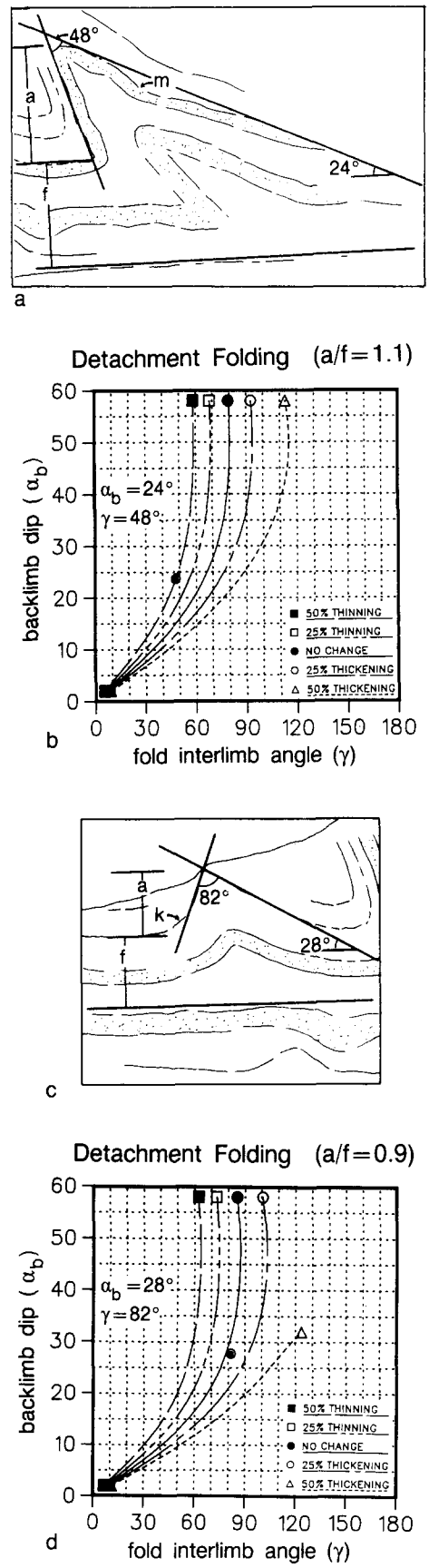

Fig. 9. Geometric analysis of Besa River folds. (a) The limbs of the right-hand fold of Fig. 8 are approximated by straight lines to determine the values needed for the geometric analysis. (b) Detachment fold charts for *a*/*f* = 1.1 suggest the outcropping fold should have forelimb thinning of 50% in the units immediately above horizon *m*. (c) Determination of the angular relationship in the left-hand fold of Fig. 8. (d) Geometric analysis indicates that this fold (*a*/*f* = 0.9) should have a slight thickening of forelimb beds at the level of horizon *k*.

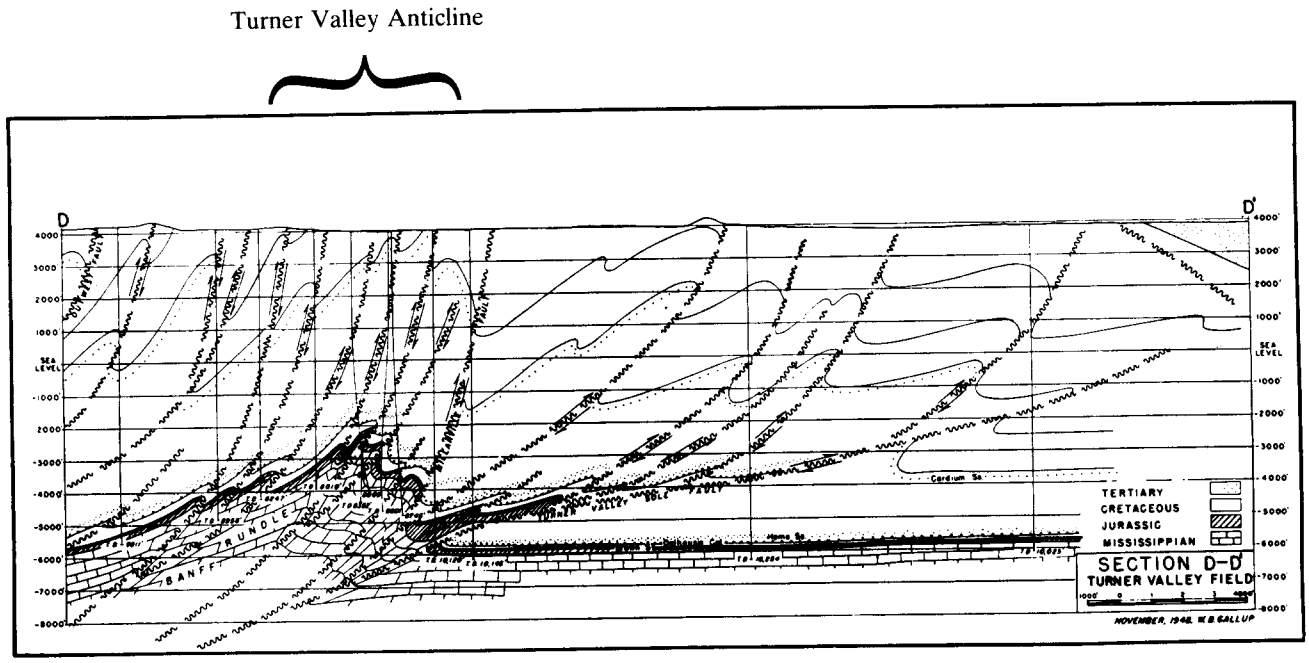

Fig. 10. Cross-sectional interpretation of the Turner Valley Anticline. Vertical to horizontal scales are 1:1. From Gallup (1951). (Reproduced with permission of American Association of Petroleum Geologists.)

larities, it should be noted that the model fold (Fig. 4b) becomes flat-topped upsection, and maintains a constant amplitude (a) throughout the folded interval. The outcropping folds do not become flat-topped, and they do not have identical amplitudes at different levels through the structure. Because of these dissimilarities, a single analysis is not appropriate for all units involved in the folding.

Subsurface example

The Turner Valley Anticline is located at the foreland limit of the Canadian Cordillera in southern Alberta (Fig. 10). Oil was discovered in the Paleozoic units of this structure in 1924, and subsequent drilling provided the data for construction of detailed cross-sections (Gallup 1951). Drilling of this structure predates the development of wire-line geophysical tools; therefore, the subsurface data consists of stratigraphic picks based on borehole cuttings.

The Turner Valley Anticline is a truncation anticline located above the ramp of the Turner Valley Sole Fault. The Mississippian units are truncated against the thrust ramp in both the hangingwall and footwall of the structure. Since both the fold and the truncated beds are located directly above the ramp of the transporting thrust fault, it can be concluded that this is a fault-propagation fold that has not been transported through the upper hinge of its associated ramp. Numerous imbricate faults are interpreted to occur throughout the Turner Valley structure (Fig. 10). One of the imbricates, the Millarville Fault, carries a separate Paleozoic fold along trend.

Geometric analysis of this structure requires more approximation than did the outcrop example simply because the structure, as interpreted, does not display smooth, planar limbs. In order to make the analysis, the forelimb, backlimb and fault ramp must be approximated by straight lines. Making these approximations (Fig. 11a), the fold interlimb angle at the top of the Mississippian carbonates is 92°, and at the top of the Cretaceous Cardium Sandstone it is 78°. Fault imbrications produce tectonic thickening in both limbs of the fold, but the thickening is greater in the forelimb. In the pre-Cardium Cretaceous units, the forelimb is about 10% thicker than the backlimb. In the Mississippian units, the relative forelimb thickening appears to be greater, although the lack of well control for basal Mississippian horizons prohibits a direct measurement of this value.

In the cross-section the ramp angle is 22°. For this ramp angle and the measured interlimb angles, the geometric analysis indicates that the Cretaceous beds should have been thickened 30% in the forelimb and the Mississippian units 45% (K_1 and M_1 in Fig. 11b). These are considerably larger amounts of forelimb thickening than depicted in the cross-section. In order to obtain folds with both the measured interlimb angles and the more modest forelimb thicknesses indicated in the cross-section, a ramp angle close to about 28° would be needed (K_2 and M_2 in Fig. 11b). As there is little control to constrain the depicted ramp angle, the section could just as easily be drawn with the larger (28°) ramp angle. Modifying the cross-section to be compatible with the geometric analysis will ensure that it is balanced.

CONCLUSIONS

Balancing techniques are the union of a belief in the conservation of matter and a suite of assumptions based upon geologic observations and simplifications. The

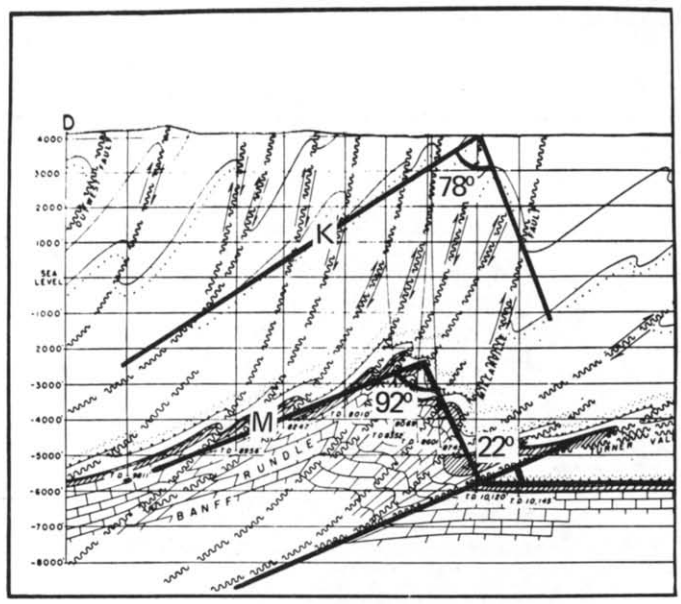

a

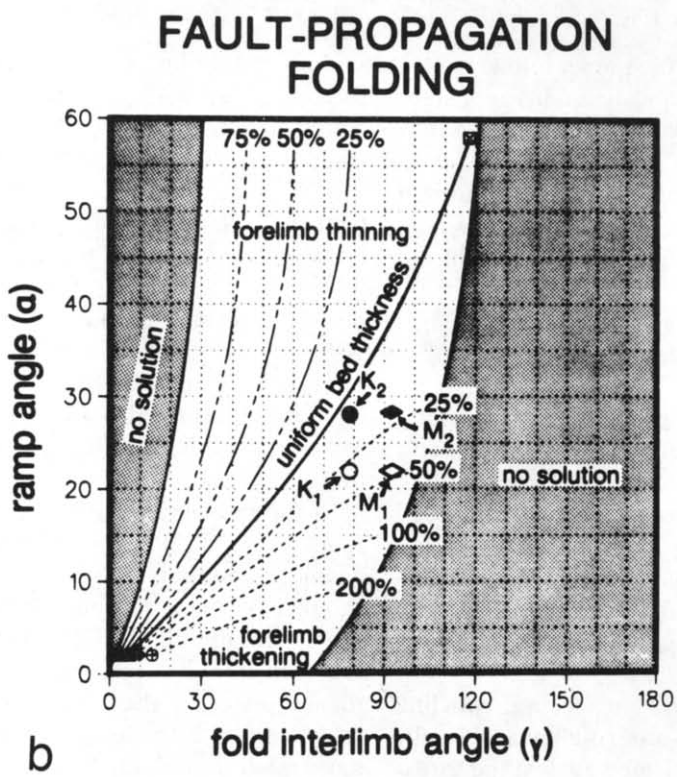

b

Fig. 11. Geometric analysis of the Turner Valley Anticline. (a) For the purposes of analysis, the fold forelimb and backlimb, the footwall bedding, and the fault are all approximated to straight lines. (b) The data from Mississippian (M_1 and M_2) and Cardium (K_1 and K_2) beds in the fold are plotted on fault-propagation fold charts relating γ and α to forelimb thickness. See text for discussion.

stated goal of the procedure dictates the chosen assumptions. The goal of this study is to relate fold geometry to the mode of fold-thrust interaction.

Fault-bend, fault-propagation and detachment folds each have a definable set of geometric associations. The most geometrically distinctive fold form is the Mode I fault-bend fold, which always has a relatively large interlimb angle. Also, tight, upright folds are more apt to be detachment folds than truncation anticlines. In general, however, there is considerable overlap and similarity of geometric solutions among the three modes of fold-thrust interaction. Consequently, determining the mode of fold development exclusively from final fold geometry is possible only for a limited suite of structures. However, the nature of the fold-thrust interaction can often be inferred by coupling the geometric analysis with

kinematic considerations, details of the deformation, and familiarity with the local geology.

The geometry and geometric relationships of a fold are altered, in a predictable fashion, when it is transported foreland through a ramp hinge. For fault-propagation folds, the alteration is such that the geometry of the transported fold is identical to the geometry of a Mode II fault-bend fold with the same ramp angle. Fault-parallel shearing of the fold during or after fold development will tighten the fold and produce a forelimb that is unusually thick for the specified fold form. Excess material that is moved into the forelimb region by the shearing produces this effect.

Geometric analysis provides a means for balancing individual folds. Application of the analysis to existing cross-section interpretations can illuminate unstated assumptions and specific weaknesses of the construction. Structural interpretations inherently require an extrapolation from the reasonably well known into the unknown. The geometric analysis can provide guidelines for this extrapolation that have a geologic foundation.

Acknowledgements—My thanks to Amoco Production Company for permission to publish this paper, which is based on a 1982 Amoco Research Department report. I am especially grateful to Martha Withjack, Ron Nelson and Dave Wiltschko for their thoughtful criticism of the manuscript.

REFERENCES

Berger, P. & Johnson, A. M. 1980. First-order analysis of deformation of a thrust sheet moving over a ramp. *Tectonophysics* **70**, T9–T24.

Boyer, S. E. & Elliott, D. 1982. Thrust systems. *Bull. Am. Ass. Petrol. Geol.* **66**, 1196–1230.

Brown, S. P. & Spang, J. H. 1978. Geometry and mechanical relationship of folds to thrust fault propagation using a minor thrust in the Front Ranges of the Canadian Rocky Mountains. *Bull. Can. Soc. Petrol. Geol.* **26**, 551–571.

Dahlstrom, C. D. A. 1969. Balanced cross-sections. *Can. J. Earth Sci.* **6**, 743–757.

Dahlstrom, C. D. A. 1970. Structural geology in the eastern margin of the Canadian Rocky Mountains. *Bull. Can. Soc. Petrol. Geol.* **18**, 332–406.

Dixon, J. S. 1982. Regional structural synthesis, Wyoming salient of western overthrust belt. *Bull. Am. Ass. Petrol. Geol.* **66**, 1560–1580.

Faill, R. T. 1969. Kink band structures in the Valley and Ridge Province, central Pennsylvania. *Bull. Geol. Soc. Am.* **80**, 2539–2550.

Fitzgerald, E. L. & Braun, L. T. 1965. Disharmonic folds in Besa River Formation, northeastern British Columbia, Canada. *Bull. Am. Ass. Petrol. Geol.* **49**, 418–432.

Gallup, W. B. 1951. Geology of Turner Valley oil and gas field, Alberta, Canada. *Bull. Am. Ass. Petrol. Geol.* **35**, 797–821.

Laubscher, H. P. 1977. Fold development in the Jura. *Tectonophysics* **37**, 337–362.

Morse, J. D. 1977. Deformation in ramp regions of overthrust faults: experiments with small-scale rock models. *Wyoming Geol. Ass. Guidebook, 29th Ann. Field Conf.* 457–470.

Rich, J. L. 1934. Mechanics of low-angle overthrust faulting as illustrated by Cumberland thrust block, Virginia, Kentucky, Tennessee. *Bull. Am. Ass. Petrol. Geol.* **18**, 1584–1596.

Serra, S. 1977. Styles of deformation in the ramp regions of overthrust faults. *Wyoming Geol. Ass. Guidebook, 29th Ann. Field Conf.* 487–498.

Suppe, J. 1980. A retrodeformable cross-section of northern Taiwan. *Geol. Soc. China Proc.* **23**, 46–55.

Suppe, J. 1983. Geometry and kinematics of fault-bend folding. *Am. J. Sci.* **283**, 684–721.

Suppe, J. & Medwedeff, D. A. 1984. Fault-propagation folding. *Geol. Soc. Am. 1984 Ann. Mtg. Prog. With Abs.* **16**, 670.

Williams, G. & Chapman, T. 1983. Strain developed in the hanging-walls of thrusts due to their slip/propagation rate: a dislocation model. *J. Struct. Geol.* **5**, 563–571.

Wiltschko, D. V. 1979a. A mechanical model for thrust sheet deformation at a ramp. *J. geophys. Res.* **84**, 1091–1104.

Wiltschko, D. V. 1979b. Partitioning of energy in a thrust sheet and implications concerning driving forces. *J. geophys. Res.* **84**, 6050–6058.

APPENDIX

The basic premises behind the geometric analyses are discussed in the text. Each model begins by equating pre- and post-deformational area of the structure. The transformation of the initial equation into the relationships used to generate the curves shown in the text is an exercise in trigonometry. In this appendix, I show only the initial and final equations.

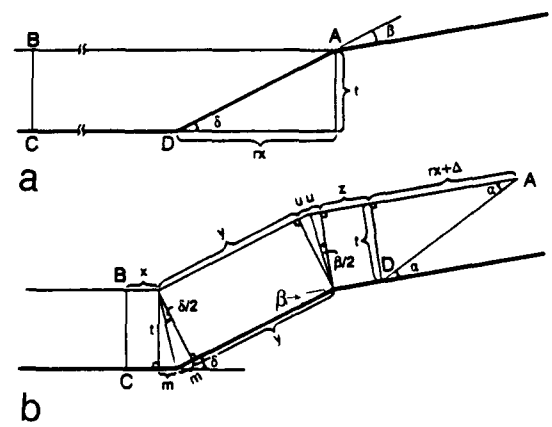

Fig. 12. Diagram for the evaluation of the effective ramp angle (α) of a fault-bend fold. (a) Fault with no offset of the hangingwall. (b) Fault after displacement of the hangingwall.

Fault-bend folding

A critical parameter in the fault-bend fold equations is the 'ramp angle' (α), which is a function of the upper and lower ramp hinge angles (β and δ, respectively). This relationship is determined by considering a transported, but unfolded, hangingwall (Fig. 12), where all units are assumed to have constant thickness. Constant cross-sectional area is maintained by keeping all bed lengths constant. From the pre-transport configuration:

$$\overline{AB} = \overline{CD} + rx. \tag{1}$$

In the post-transport configuration, this becomes:

$$x + y + 2u + z + rx + \Delta = x + 2m + y + z + rx, \tag{2}$$

or

$$\Delta = 2m - 2u, \tag{3}$$

which leads to:

$$\cot \alpha = \cot \delta + 2[\tan (\delta/2) - \tan (\beta/2)]. \tag{4}$$

The fault-bend fold is formed by allowing the leading-edge triangle of the hangingwall block to rest against the underlying thrust (Fig. 13). In so doing the forelimb of the fault-bend is formed. The bedding-normal thickness of this leading edge triangle (tf) is not required to equal the original bedding thickness (t). The pre- and post-folding geometries are equated as:

$$\text{area } \Delta ABD = \text{area } \Delta ABC + \text{area } \Delta ACE \tag{5}$$

which yields

$$\cot \alpha = \cot \gamma_1 + \sin \gamma_2/[\sin \gamma_1 \sin (\gamma_1 + \gamma_2)]. \tag{6}$$

Note that here, and in all ensuing models, the forelimb to backlimb thickness ratio may be expressed as:

$$tf/t = \sin \gamma_2/\sin \gamma_1. \tag{7}$$

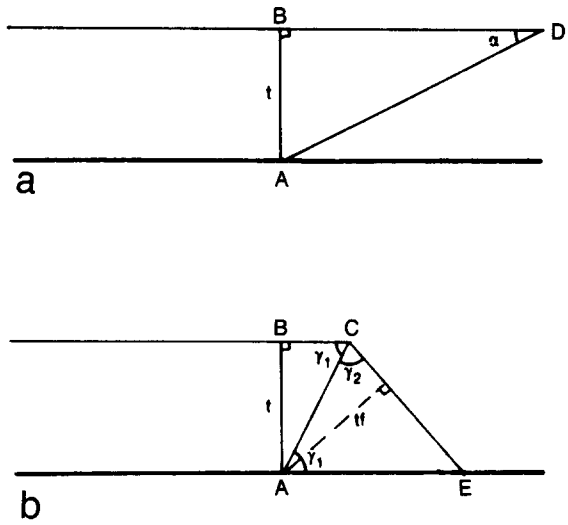

Fig. 13. Diagram for evaluation of fold interlimb angle of a fault-bend fold for a given α. (a) Prefolding and (b) post-folding geometries.

Fault-propagation folding

Separate geometries and equations are assigned to those units in contact with the fault versus those not in contact with the fault (Fig. 14). The ramp angle in this fold-thrust model is the lower ramp hinge angle. For those units in contact with the fault, the equated pre- and post-folding areas are expressed as:

$$\text{area } \Delta ABC = \text{area } \Delta ABF + \text{area } \Delta AFC, \tag{8}$$

which yields:

$$\cot \alpha = 2 \cot \gamma_1 - \tan \phi - \cot \gamma. \tag{9}$$

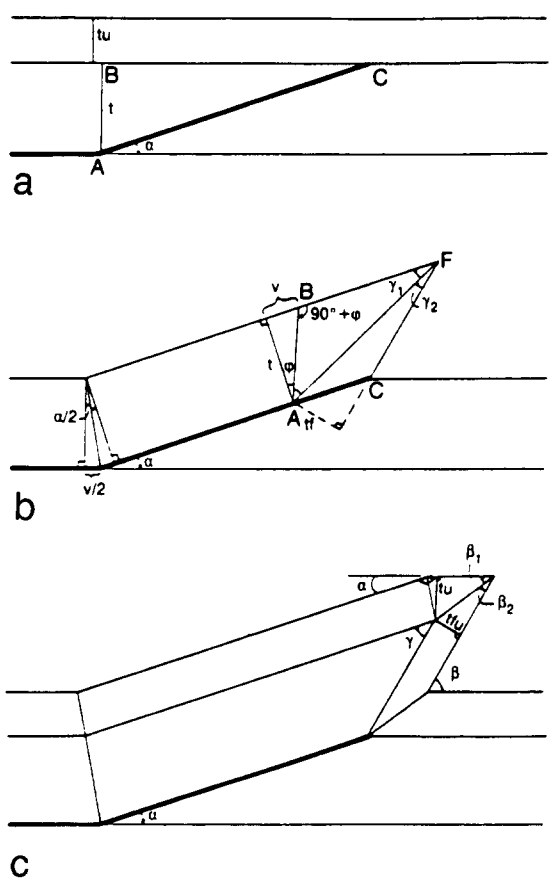

Fig. 14. Diagram for evaluation of fault-propagation fold. (a) Unfolded units. (b) Folded unit in direct contact with the propagating fault. (c) Folded unit not in contact with propagating fault.

Noting that:

$$\tan \phi = 2 \tan (\alpha/2), \tag{10}$$

the preceding equation may be written as:

$$\gamma = \gamma_1 + \gamma_2 + \tan^{-1} [1/(2 \cot \gamma_1 - (2 - \cos \alpha)/\sin \alpha)]. \tag{11}$$

For those units not in contact with the fault (Fig. 14c), the model is constructed such that:

$$\beta = \beta_1 + \beta_2 = \gamma + \alpha. \tag{12}$$

Using the assumption that:

$$tfu/tu = tf/t \tag{13}$$

leads to:

$$\beta_1 = \tan^{-1} [(2 \sin \alpha)/(2 \cos \alpha - 1)]. \tag{14}$$

The geometric relationships for the fault-propagation fold are defined by those units in contact with the fault.

Detachment fold

The chevron fold form used in this paper is a degenerative case of the more general box-fold geometry (Fig. 15). The basic geometric relationships come from analysis of the 'ductile' unit in the core of the fold. The pre-folding area (Fig. 15a) is:

$$A_1 = \text{area } ABCD = fL_o, \tag{15}$$

where:

$$L_o = e_1(t/tf) + e_2 + e_3. \tag{16}$$

The post-folding area (Fig. 15b) is:

$$A_2 = \text{area } ABCD + \text{area } ADGH. \tag{17}$$

Equating these pre- and post-folding areas yields:

$$a/f = \frac{[t/(tf \cos \beta) + (1/\cos \delta) - \tan \beta - \tan \delta]}{[e_2/a + \frac{1}{2}(\tan \beta + \tan \delta)]}. \tag{18}$$

Allowing thickness changes to occur in the forelimb of the stiff unit, it is found that:

$$tf/t = \cos \beta \cot \xi_1 + \sin \beta. \tag{19}$$

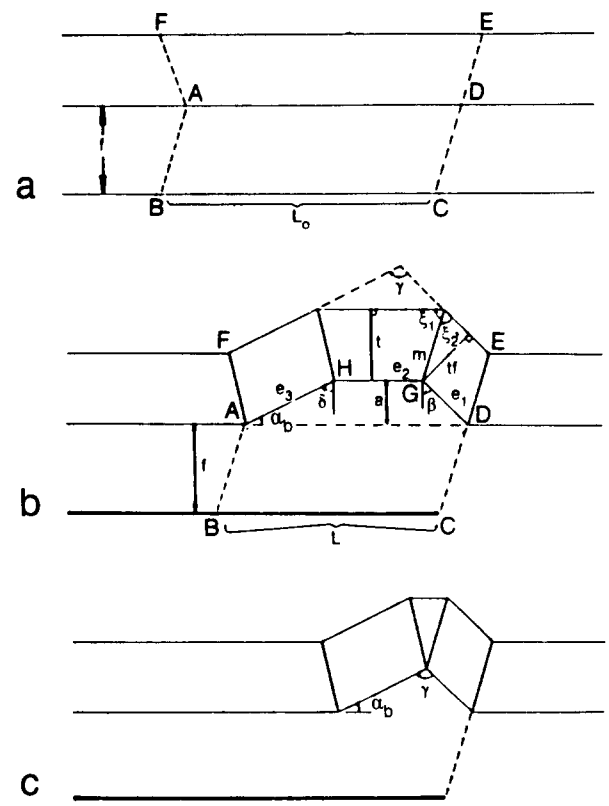

Fig. 15. Diagram for evaluation of detachment folds. (a) Units before folding. (b) General detachment fold (box fold) after folding. (c) Chevron fold form.

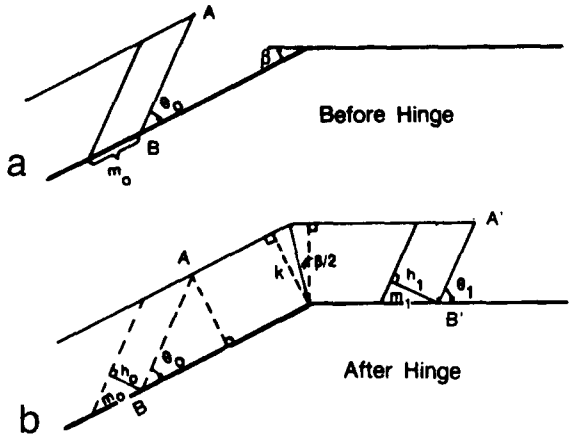

Fig. 16. Diagram for evaluation of the effect of upper ramp hinge on fold interlimb angle and forelimb thickness. (a) Pre-transport and (b) post-transport configuration.

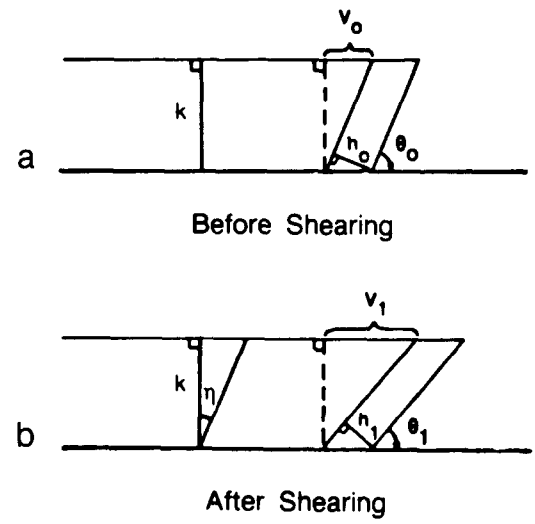

Fig. 17. Diagram for evaluation of the effect of fault-parallel shear on fold interlimb angle and forelimb thickness. (a) Pre-shearing and (b) post-shearing configuration.

The chevron geometry (Fig. 15c) is achieved simply by letting e_2 go to zero. Using α_b as backlimb dip in this model, and noting that:

$$\alpha_b = 90° - \delta \quad \text{and} \quad \gamma = \beta + \delta \tag{20}$$

then:

$$a/f = 2(t/tf \sin \alpha_b/\sin \gamma + \cos \alpha_b + \sin \alpha_b \cot \gamma - 1). \tag{21}$$

Transport through an upper ramp hinge

For this calculation, it is assumed that there is no change in thickness of the structure, measured perpendicularly to the fault, during the transporting process (Fig. 16). Consequently, transport distances for the top and bottom surfaces of the structure are equal, i.e.:

$$\overline{AA'} = \overline{BB'}. \tag{22}$$

This observation allows pre- and post-transport angles to be related by:

$$\tan \theta_1 = \tan \theta_0/[1 - 2 \cdot \tan \theta_0 \cdot \tan (\beta/2)], \tag{23}$$

where the angles are measured relative to the fault surface. If θ_0 and θ_1 are bedding surface measurements, the post-transport thickness of this bed (h_1) relative to its initial thickness (h_o) is:

$$h_1/h_o = \sin \theta_1/\sin \theta_0. \tag{24}$$

Transport through a lower ramp hinge reverses the position of the variables.

Fault-parallel shearing

Uniform, fault-parallel shear through an angle η (Fig. 17) produces roughly the opposite effect as transport through an upper ramp hinge. Here:

$$\tan \theta_1 = \tan \theta_0/(1 + \tan \theta_0 \tan \eta) \tag{25}$$

and, as before:

$$h_1/h_o = \sin \theta_1/\sin \theta_0. \tag{26}$$